Renewable and Sustainable Energy Reviews 141 (2021) 110747

Contents lists available at ScienceDirect

Renewable and Sustainable Energy Reviews

journal homepage: http://www.elsevier.com/locate/rser

Effects of depth-cycling on nutrient uptake and biomass production in the giant kelp *Macrocystis pyrifera*

Ignacio A. Navarrete [a,1], Diane Y. Kim [a,b,*,1], Cindy Wilcox [c], Daniel C. Reed [d], David W. Ginsburg [a,b], Jessica M. Dutton [a,b], John Heidelberg [a,b,e], Yubin Raut [e], Brian Howard Wilcox [c]

[a] *Wrigley Institute for Environmental Studies, University of Southern California, Los Angeles, CA, 90089, USA*
[b] *Environmental Studies Program, University of Southern California, Los Angeles, CA, 90089, USA*
[c] *Marine BioEnergy, Inc., La Cañada, California, 91011, USA*
[d] *Marine Science Institute, University of California at Santa Barbara, Santa Barbara, CA, 93106, USA*
[e] *Biological Sciences, University of Southern California, Los Angeles, CA, 90089, USA*

ARTICLE INFO

Keywords:
Biofuel
Kelp
Depth-cycling
Nutrients
Open-ocean
Mariculture
Macroalgae

ABSTRACT

Seasonal or chronic nutrient limitations in the photic zone limit large-scale cultivation of seaweed (macroalgae) in much of the world's oceans, hindering the development of macroalgae as a biofuel feedstock. One possible solution is to supply nutrients using a diel depth-cycling approach, physically moving the macroalgae between deep nutrient-rich water at night and shallow depths within the photic zone during the day. This study tested the effects of depth-cycling on the growth, morphology, and chemical composition of the giant kelp *Macrocystis pyrifera*, a target species for renewable biomass production. Giant kelp grown under depth-cycling conditions had an average growth rate of 5% per day and produced four times more biomass (wet weight) than individuals grown in a kelp bed without depth-cycling. Analysis of tissue from the depth-cycled kelp showed elevated levels of protein, lower C:N ratios, and distinct $\delta^{15}N$ and $\delta^{13}C$ values suggesting that the depth-cycled kelp were not nitrogen-deficient and assimilated nutrients from deep water. Depth-cycled kelp also exhibited smaller and thicker-walled pneumatocysts and larger blades. Overall, this study supports further investigation of depth-cycling as a macroalgal farming strategy.

1. Introduction

Global climate change caused by the accumulation of anthropogenic greenhouse gases has created an urgency to develop renewable energy alternatives [1,2]. Biofuels developed from primary producers are an attractive choice because of their potential to be carbon neutral – carbon dioxide is released when biofuels are burned but is also removed from the atmosphere during feedstock growth. Furthermore, biofuels are compatible with existing infrastructure, and are the only low-carbon fuels with the energy density required for transportation over long distances [3]. Unfortunately, current biofuel feedstocks have significant drawbacks. In particular, farming and fertilization of biofuel crops is often carbon intensive, and the expansion of terrestrial biofuel crops may come at the expense of food crops or other vegetation and compete for land and fresh water [4]. The use of marine macroalgae (or seaweed) feedstocks circumvents these issues and thus represents a promising alternative [5,6]. Compared to terrestrial feedstocks, the lack of ligno-cellulose in brown macroalgae also simplifies the conversion of biomass into fuel [7]. Considering the vast expanse of the world's ocean, the potential for large-scale ocean farming of macroalgae seems plausible and should be considered as a potential sustainable and cost-effective source of renewable biofuel feedstock.

Recognizing the potential to decrease dependence on fossil fuels, the U.S. Department of Energy's Advanced Research Projects Agency-Energy (ARPA-E) recently invested $22 M to develop mechanisms to increase marine biomass production through the Macroalgae Research Inspiring Novel Energy Resources (MARINER) program. Macroalgae were previously explored as a biofuel feedstock in the U.S. during the 1970–80s under the Ocean Food and Energy Project [8] and Marine Biomass Program [9], which greatly advanced our understanding of both the potential and challenges of developing this resource. These

* Corresponding author. Wrigley Institute for Environmental Studies, University of Southern California, Los Angeles, CA, 90089, USA.
E-mail address: dianekim@usc.edu (D.Y. Kim).
[1] These authors contributed equally to this work.

https://doi.org/10.1016/j.rser.2021.110747
Received 14 May 2020; Received in revised form 15 January 2021; Accepted 17 January 2021
Available online 19 February 2021

List of abbreviations

ANOVA	Analysis of Variance
ARPA-E	Advanced Research Projects Agency-Energy
B-E	Buoy-Elevator
BEUTI	Biologically Effective Upwelling Transport Index
BFC	Big Fisherman's Cove
C	Carbon
CF-IRMS	Continuous Flow Isotope Ratio Mass Spectrometry
CTD	Conductivity Temperature Depth
CUTI	Coastal Upwelling Transport Index
DMSO	Dimethyl Sulfoxide
GAM	General Additive Model
MARINER	Macroalgae Research Inspiring Novel Energy Resources
MLD	Mixed Layer Depth
N	Nitrogen
PAR	Photosynthetically Active Radiation
PL	Parsons Landing
PVC	Polyvinyl Chloride
SCB	Southern California Bight
SBE	Sea Bird Electronics
SST	Sea-Surface Temperature
Stdev	Standard deviation
WMSC	Wrigley Marine Science Center

programs were eventually discontinued in an environment of low oil prices; however, there is now a renewed worldwide interest in macroalgal fuels [10,11]. Several viable pathways for the conversion of biomass into fuels [12] currently exist and include hydrothermal liquefaction, which generates a bio-crude from wet biomass that can be processed using existing refinery technology and fed into traditional distribution channels, thus eliminating the need for new infrastructure. Accordingly, the limiting factor in developing macroalgae as a biofuel feedstock is the need for large-scale and year-round production of marine biomass at a price comparable to terrestrial bioenergy feedstocks and fossil fuels.

Giant kelp, *Macrocystis pyrifera* (Laminariales), has long been considered one of the most promising macroalgal species for biomass production due to its large size, rapid growth rates, and life cycle strategies. *Macrocystis* is commonly found in temperate subtidal marine ecosystems where it forms a dense underwater habitat, and can grow at a rate of up to 35 cm per day [13]. Mature individuals are capable of producing hundreds of fronds (the entirety of a single stipe and all its associated blades) that are constantly turning over, with older longer fronds senescing and shorter new fronds forming near the base or holdfast of the individual [14]. This growth pattern allows for the harvest of biomass from older fronds while individuals continue producing new fronds (for one to several years), potentially increasing the efficiency of production cycles. Fronds can reach lengths of over 30 m [15], often forming large floating canopies at the sea surface (the result of pneumatocysts, gas-filled vesicles that develop at the base of all non-reproductive blades). Additionally, the life history of *Macrocystis* includes a haploid gametophyte stage that is easily maintained and cultured in the laboratory, allowing for the development of a germplasm bank of known genotype and phenotype [16].

While the ocean offers a large area for potential cultivation (the U.S. Exclusive Economic Zone alone spans >11 million km^2), there are significant challenges to growing macroalgae in deep open-ocean environments [17]. The distribution of giant kelp is confined to cool temperate seas and is restricted by the availability of light, nutrients, and hard substrate for attachment, limiting its growth to shallow reefs that experience seasonal upwelling. Giant kelp are typically found at depths of 5–20 m, though they have been found in deeper depths where conditions allow for deeper light penetration [18]. In contrast, the average depth of the open ocean is ~4000 m, with the photic zone limited to the upper ~100–300 m and the majority of photosynthetically active radiation (PAR) within 50 m of the surface [19]. In the open ocean, nutrient concentrations are typically very low near the surface due to rapid uptake by phytoplankton, but then increase with depth below the photic zone as organic matter is re-mineralized [20]. Deep water has been shown to provide the key nutrients for *Macrocystis* growth [21]. Consequently, cultivation of kelp in the open ocean requires both an artificial substrate to maintain the kelp within the upper photic zone and some mechanism to deliver deep-water nutrients.

A possible solution to surface nutrient limitation is the development of depth-cycling farms that submerge kelp to nutrient-rich deep water at night and surface kelp to shallower sunlit depths during the day. The success of such farms would rely on the ability of species such as *Macrocystis* to thrive under depth-cycling conditions. In particular, giant kelp would have to tolerate substantial daily changes in pressure during each transition between shallow and deep water which could damage its gas-filled pneumatocysts [22] and have other detrimental physiological consequences. Kelp would also need to assimilate nutrients in the absence of light, a metabolic process that appears to be either dependent on or facilitated by light in some macroalgal species [23–27], but not others [28].

Here, we describe the results from an *in situ* experiment testing the biological response of *Macrocystis* to daily depth-cycling between nutrient poor surface waters and nutrient rich deeper water. Depth-cycling was accomplished using an anchored buoy-elevator system which cycled the kelp between ~9 m and ~80 m daily for 90 days. Results from the experiment demonstrated that the amount of *Macrocystis* biomass produced under daily depth-cycling conditions was significantly greater than individuals from a natural kelp bed, and warrant further consideration of depth-cycling as a macroalgal farming strategy.

2. Methods

2.1. Experimental sites

Three experimental sites were established in the waters off Santa Catalina Island (Figs. 1A-C and 2), located 20 miles offshore from Los Angeles in the Southern California Bight (SCB): 1) An automated Buoy-Elevator (B-E) installation in relatively deep water (169 m) used to test the biological response of *Macrocystis* to depth-cycling, 2) a fixed installation on the benthos (~9 m) on the northern edge of a kelp bed at Parsons Landing (PL) used for comparison of depth-cycled kelp to kelp grown in its natural habitat, and 3) a fixed-depth installation (9 m) at Big Fisherman's Cove (BFC, max depth ~20 m) where kelp were suspended in the water column as is typical of current kelp mariculture operations. Though the *in situ* nature of this study precluded traditional controls, PL and BFC serve as comparative sites to the B-E. All three sites are located within the SCB and thus experience similar mesoscale conditions characteristic of this region, but also display unique characteristics described below.

B-E (33°28′12.78″N, 118°29′33.30″W) is a sandy bottom site approximately 169 m deep, located ~3 km north of the town of Two Harbors on Catalina Island and exposed to currents and swell conditions in the San Pedro Channel (Fig. 2) [29,30]. The B-E site was chosen for depth-cycling as an accessible location subject to open-ocean like conditions with low concentrations of nutrients at the surface and high concentrations below the thermocline [20]. A 2.5 m diameter buoy equipped with a solar-powered winch was moored at the site to raise and lower a submerged tetrahedron structure consisting of fiberglass beams

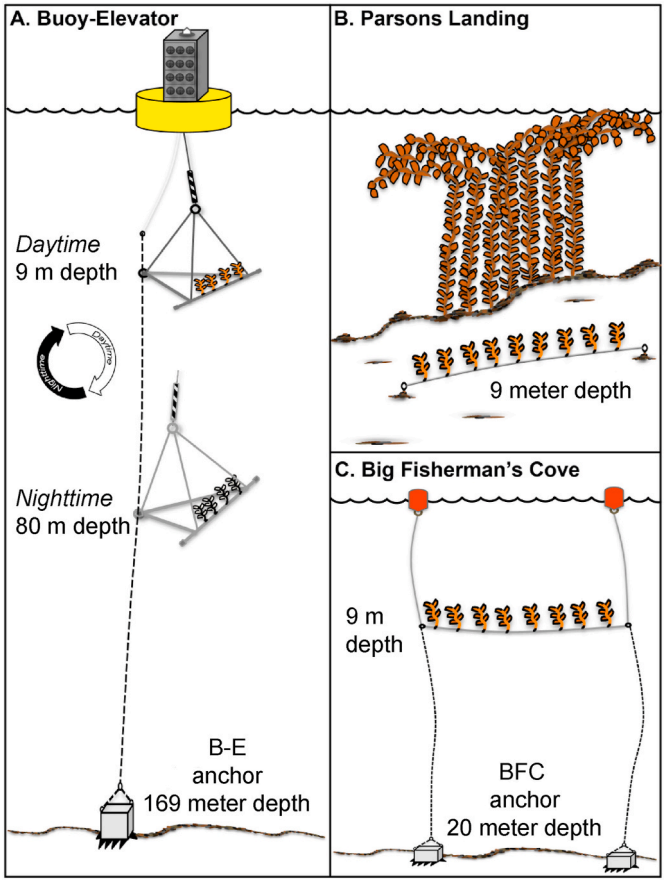

Fig. 1. Experimental sites. (A) The Buoy-Elevator (BE) experimental platform depth-cycled kelp between 9 m during the day and 80 m at night. (B) Parsons Landing (PL) was the site of collection for all the kelp used in the trial and also used as a reference for growth of kelp in its natural setting. Experimental kelp were outplanted at the edge of a naturally occurring kelp bed. (C) Kelp were outplanted along a polypropylene rope that was suspended at 9 m in the water column at Big Fisherman's Cove (BFC), mimicking established near-shore farming practices.

suspended from stainless steel cables at a rate of 7 cm sec^{-1} (Fig. S1). The longest side of the tetrahedron is 12 m and was used as the attachment point for PVC pipes populated with wild-collected juvenile *Macrocystis* used for the depth-cycling trial. The winch was programmed to raise and lower the tetrahedron between ~9 m and ~80 m daily at 0500 and 1900 Pacific Time, respectively (Fig. 1A).

PL (33°28′25.5″N 118°33′06.3″W) is a rocky subtidal reef located near the western end of Catalina Island that commonly harbors *Macrocystis* [31] (Fig. 2). Typical Southern California kelp forest herbivores such as sea urchins, abalone, and snails can be found at this location. PL was the collection site for juvenile kelp used at all experimental sites, and transplants back to PL were used to compare the growth, survival, and chemical composition of depth-cycled kelp at B-E to individuals grown in their native habitat. To secure the transplanted kelp at PL, two eyebolts were attached onto rocks using Z-Spar underwater epoxy and placed ~30 m apart from each other at a depth of ~9 m at the western edge of a naturally occurring kelp bed (Fig. 1B). A 3-mm lead (Pb) line was secured to the eyebolts and served as the attachment point for horizontal PVC pipes populated with juvenile giant kelp transplants.

BFC (33°26′41.8″N 118°29′08.5″W) is located inside the Blue Cavern Onshore State Marine Conservation Area and relatively sheltered from swell and current conditions [32] (Fig. 2). BFC was used to assess the growth of kelp transplanted to a shallow fixed depth suspended in the water column. The experimental site in BFC is a sandy bottom environment with a depth of ~20 m. Approximately 18 m of

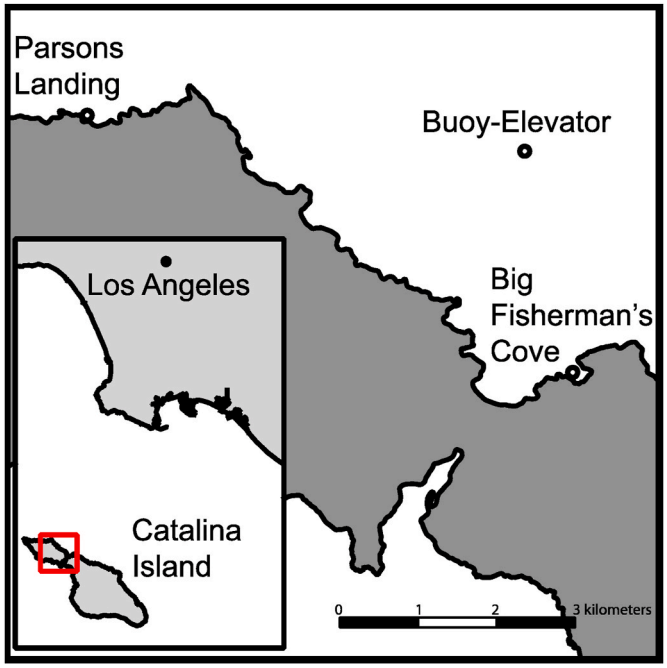

Fig. 2. Study location. The study was conducted on the north side of Santa Catalina Island's isthmus in the SCB (eastern North Pacific) (inset) and included three sites: BFC, PL, and B-E (see Fig. 1).

polypropylene line was secured using two moorings at a depth of ~9 m to match the 'surface' depth at the B-E site (Fig. 1C). Situated inside a marine reserve, BFC typically harbors similar vertebrate and invertebrate species as found at PL, but since kelp were suspended in the water column at this site they were presumably not accessible to benthic species.

2.2. Environmental conditions

The primary goal of this study was to assess the growth of giant kelp when depth-cycled under conditions where nutrients are limiting at the surface but not at depth. To determine nutrient availability, we used a combination of direct measurements of inorganic nitrogen (nitrate, nitrite, ammonia) and phosphate from seawater samples taken from different depths, as well as temperature measurements, which can be used to determine thermocline depth [33] and estimate nitrate concentrations [34]. Water samples and hydrographic water column profiles (measuring conductivity, temperature, and dissolved oxygen) were collected at potential depth-cycling study site locations prior to the start of the experiment (Fig. S2, Tables S1 and S2), as well as collected twice at each kelp outplant site during the experiment (Table 1). These measurements were later used to model the relationship between temperature and nitrate concentration. Temperatures were also recorded at each outplant site during the experiment using continuous data loggers places underwater. Combining these data with our model of the relationship between temperature and nitrate allowed us to estimate ambient nitrate concentrations at each site throughout the experiment.

Hydrographic profiles were collected using a Sea Bird Electronics (SBE) 25plus Sealogger with Conductivity, Temperature, and Depth (CTD) sensors together with a SBE43 Dissolved Oxygen sensor with all sensors recording at a rate of 16 samples per second. Measurements were made onboard a 25-ft vessel, lowering and raising the CTD sensor package using a power hauler at a rate of about 1 m sec^{-1}. Raw CTD and oxygen sensor files were processed by the Southern California Marine Institute using the SBE Data Processing software. Mixed Layer Depths (MLD) were calculated using a temperature threshold criterion of sea-surface temperature (SST) – 0.8 °C [35] which performed well in

Table 1
Hydrographic data at the three experimental sites on multiple dates and depths relevant to the study. bd = below detection; nd = no data.

Site	Date	Depth	Nitrate	Nitrite	Ammonia	Phosphate	Temperature	Salinity	Dissolved Oxygen
	m d^{-1} y^{-1}	m	μM	μM	μM	μM	°C	ppt	mL L^{-1}
B-E	5/9/2019	10	0.58	bd	nd	0.44	16.73	33.63	5.61
		30	3.57	0.26	nd	0.75	14.63	33.63	5.52
		50	11.72	0.19	nd	1.30	11.96	33.66	4.10
		70	15.41	bd	nd	1.60	10.91	33.71	3.55
		100	20.96	bd	nd	2.04	10.06	33.84	2.90
	6/18/2019	10	bd	bd	bd	0.14	16.62	33.81	6.05
		30	11.20	0.27	bd	1.13	12.22	33.71	4.19
		50	18.20	0.11	bd	1.54	10.81	33.74	3.28
		70	22.50	0.10	bd	1.84	10.34	33.82	2.84
		100	25.50	0.12	bd	2.05	9.76	33.96	2.38
	7/25/2019	10	bd	bd	bd	0.16	19.89	33.85	5.21
		30	1.12	bd	bd	0.38	16.24	33.78	5.72
		50	10.60	0.26	bd	1.09	12.38	33.85	4.45
		70	18.30	bd	bd	1.52	11.15	33.83	3.34
		100	17.10	bd	bd	1.55	10.06	33.92	2.54
PL	6/18/2019	5	0.41	0.13	bd	0.26	16.96	33.68	5.76
		8	3.16	0.19	bd	0.55	15.75	33.79	5.91
	7/25/2019	5	bd	bd	bd	0.11	18.86	33.76	5.59
		8	bd	bd	bd	0.17	18.43	33.71	5.75
BFC	6/18/2019	5	0.37	bd	bd	0.22	17.95	33.70	5.65
		10	1.94	bd	bd	0.35	17.42	33.79	5.64
		15	2.51	0.18	bd	0.50	15.75	33.74	5.28
	7/25/2019	5	bd	bd	bd	0.14	19.84	33.75	5.52
		10	0.57	bd	bd	0.30	17.93	33.81	5.70
		15	0.87	bd	bd	0.28	16.81	33.71	5.72

estimating MLD in the California Current [33] where the B-E site is located.

Seawater samples were collected from discrete depths using a 2 L Niskin bottle (General Oceanics) during each sampling cruise. Sampling depths (Tables S2 and 1) were chosen to maximize coverage of the relevant portion of the water column, as each site varied in maximum depth. Seawater collected from each depth was syringe filtered through a 0.2 μm filter (Corning™ Polyethersulfone Syringe Filters, Fisher Scientific) into 20 mL scintillation vials, immediately frozen on dry ice, and stored at −20 °C until further processing. Seawater samples were analyzed by the University of California Santa Barbara's Marine Science Institute Analytical Lab for Nitrite, Nitrite plus Nitrate, Ammonia, and *Ortho*-phosphate concentrations using Flow Injection Analysis on a QuikChem 8500 Series 2 (Lachat Instruments, Zellweger Analytics). Nitrate-depth profiles were also estimated using a nitrate-temperature regression (see below), and nutricline depths (ND) were estimated as the depth where estimated nitrate concentrations were 1.025 μM [36].

High frequency temperature data in combination with a relationship between temperature-nitrate and upwelling models were used to assess nutrient exposure at each site during the course of the experiment. Temperature data was collected using a combination of Onset HOBO Pendant Temperature/Light Loggers (part# UA-002-08), HOBO Pendant MX Temperature/Light Data Loggers (part# MX2202) and HOBO TidbiT MX Temperature 5000′ Data Loggers (part# MX2204) logging every 15 min (B-E and PL) or 1 h (BFC). Loggers at B-E and PL were installed immediately adjacent to outplanted kelp, while the temperatures collected for the BFC site were taken from loggers previously installed by the USC Catalina Conservation Divers (https://dornslife.usc.edu/wrigley/wies-ccd/) at a site ~200 m northwest of the installation and a depth of 9 m. There were missing data between 6/20/2019 and 7/28/2019 for PL due to failed loggers.

Hydrographic profiles and nitrate measurements from seawater samples collected at and near the B-E site (Table S2) were used to model the relationship between temperature and nitrate for the study area. Following Snyder et al. [34] a Generalized Additive Model (GAM) was fit to this temperature and nitrate dataset using the mgcv package in R with the restricted maximum likelihood method (k = 10, family: gaussian, link function: identity) [37]. The temperature-nitrate GAM was then used to predict instantaneous nitrate concentrations for each time point from high-frequency temperature data obtained from the *in situ* loggers, which were then averaged to give mean daily nitrate concentrations. Two new upwelling indices that improve upon classical upwelling indices (e.g. Bakun Index) for the U.S. west coast (33 °N) were used to assess the influence of upwelling at all three sites [38]. The Biologically Effective Upwelling Transport Index, BEUTI, an estimate of vertical nitrate flux and Coastal Upwelling Transport Index, CUTI, an estimate of vertical transport are publicly available datasets [39].

2.3. Experimental design

To test the effects of depth-cycling on *Macrocystis* growth and morphological response, juvenile giant kelp were transplanted to each of the three sites. On May 13, 2019, about 120 young *Macrocystis* individuals (~25 cm in length and single bladed or recently-split double-bladed without pneumatocysts) were hand collected from PL at depths between 6 and 12 m by divers using SCUBA and then transferred to flow-through seawater tables at the USC Wrigley Marine Science Center (WMSC) on Catalina Island. Individual kelp outplants were each assigned an ID number, measured, weighed, and photographed before being randomly assigned to one of the three experimental sites (35 individuals at BFC and B-E, 40 at PL). The weights and lengths of each outplant assigned to the three sites were not significantly different (Kruskal-Wallis test; wet weights: H = 2.631, df = 2, P = 0.268; lengths: H = 0.657, df = 2, P = 0.720). Tissue samples from six additional juveniles were dried for elemental analysis (see Tissue composition section below).

The following day (experimental day 0), tagged individuals were transported to each experimental site in coolers filled with seawater. Outplants were deployed at each site using 1.5-m long ½"-PVC pipes as the substrate. The PVC pipes were sanded and incubated in flow-through seawater tanks for several days prior to use in order to 'season' them. For attachment, kelp stipes were spliced into a 12-cm piece of three-strand ¼" polypropylene rope. Cable ties were woven into the rope at each end flanking the kelp and were used to attach the kelp to the PVC pipes with 30 cm spacing for a total of 5 kelp plants per pipe. Four ¼" holes were pre-drilled along the PVC pipe to secure them to the experimental structures at each site using heavy-duty zip-ties.

Kelp outplanted at the B-E site was depth-cycled for 90 of the 107

days between kelp transplant and recovery, with interruptions caused by large swells and technical glitches occasionally preventing cycling (Table S3). On day 104 of the experiment, the tetrahedron platform at B-E descended to the sea floor due to a compromised cable-eye. The following day, the tetrahedron and attached kelp were recovered and towed underwater to BFC at a speed of <2 km hr^{-1}, where it was then attached to a mooring and maintained at a depth of ~10 m. Two days later, 107 days after outplanting, the attached B-E kelp were recovered from the tetrahedron via SCUBA and transported to the lab at WMSC for analysis. Kelp outplants at PL were recovered on day 113 and at BFC on day 119.

2.4. Growth and morphology

In-situ growth measurements and photography were conducted by SCUBA divers throughout the experiment to monitor kelp growth and development. During the transition from juvenile to adult, the overall morphology of *Macrocystis* changes substantially which required a shift from measurements of overall length to measuring the length of each stipe and finally the number of stipes achieving 1 m or greater in length (Fig. 3A and B).

The overall length of each kelp plant (as measured from the base of the primary stipe to the furthest blade tip) was used as the metric for growth for the first 42 days (Fig. 3A). Five individuals at PL and 4 at B-E were completely lost within this period and excluded from our analysis. An additional 3 individuals at B-E had one or more missing time-points due to challenging diving conditions at that site and were also excluded. Following observations of primary dichotomous branching and frond development, up to four different stipes were tagged and measured for each outplant to determine stipe elongation rates (cm per day). Stipe lengths were measured as the distance between the base of the primary stipe (where it attaches to the holdfast) and the apical meristem (Fig. 3B). Stipe lengths were measured *in-situ* at B-E on July 15 and PL on July 18 and upon recovery (see below). After further growth, stipe lengths at B-E were too long to accurately measure *in-situ* so the number of stipes greater than 1 m was counted for each individual at PL and B-E on August 8 (87 days) and August 11 (90 days), respectively.

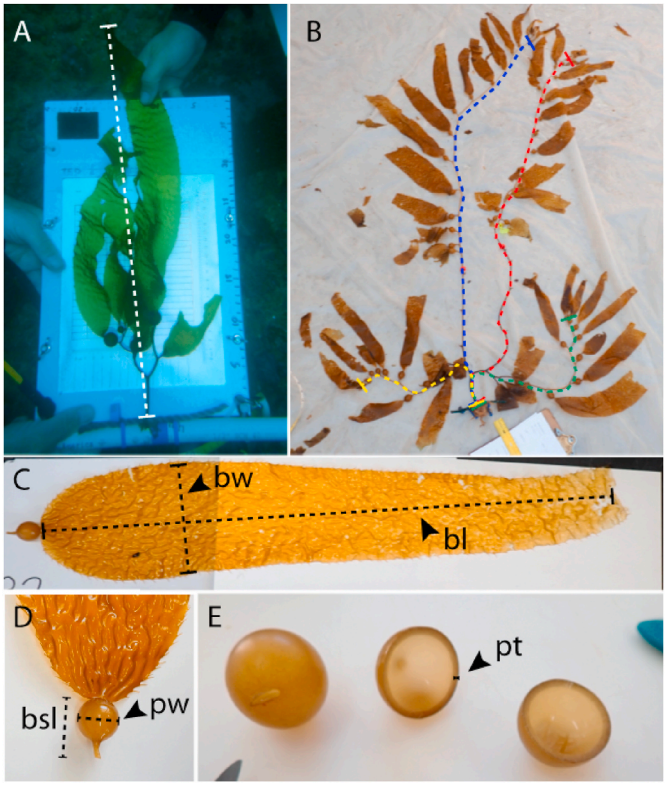

Fig. 3. Morphological measurements. (A) Overall length measurement of juvenile kelp. (B) Measurements of stipe length (each color corresponds to a single stipe measurement). (C) Blade size measurements; length (bl) and width (bw). (D, E) Pneumatocyst measurement; blade stem length (bsl), pneumatocyst width (pw) and pneumatocyst wall thickness (pt).

At the end of the experiment, recovered kelp were measured and photographed including a detailed analysis of pneumatocyst and blade morphology (Fig. 3B–E). Wet weights were determined using a motion compensating load cell (RL20000 ST) from Rice Lake. Percent growth per day was calculated using the equation

$$r = \frac{(\ln(W_2) - \ln(W_1))}{t_2 - t_1}$$

where r is relative growth per day and W_1 and W_2 are individual wet weights at times t_1 (deployment) and t_2 (recovery). Individuals were placed on a white plastic sheet and photographed, and the length of each stipe was recorded.

Previously tagged stipes with intact apical meristems were used to calculate the rate of elongation for each individual stipe in cm per day and the relative elongation rate (RER) using the equation

$$RER = \frac{(\ln(L_2) - \ln(L_1))}{t_2 - t_1}$$

where L_1 and L_2 are stipe lengths at times t_1 and t_2. Thirty individuals were recovered from B-E and 27 from PL. There were no intact individuals at the BFC site with only the holdfasts and small portions of stipe still present. The presence of apparent sorus tissue on individuals transplanted to B-E was photographed but not quantified, and no sorus tissue was observed on kelp transplanted to PL or BFC. Two or three mature blades were harvested from 14 individuals recovered from PL and B-E (each) by severing the blade stem at the point of intersection with the stipe. Blades were photographed, pneumatocysts removed for measurement, and ~10 g and ~20 g pieces of tissue removed for pigment and elemental/isotopic analysis, respectively. Tissue for pigment analysis was immediately frozen on dry ice, while tissue for elemental/isotopic analysis was dried overnight at 60° C. The remaining tissue was air dried on lines in a research greenhouse for proximate analysis. The maximum width of each pneumatocyst, as well as the blade stem length (Fig. 3D), was measured using calipers. Pneumatocysts were bisected at their widest point using a scalpel to allow measurement of the pneumatocyst wall thickness (Fig. 3E). Any indications of damage and the presence or absence of fluid within each pneumatocyst was also recorded. Blade lengths and widths were measured using photographed images that included a length reference using ImageJ software (https://fiji.sc/) (Fig. 3C).

2.5. Tissue composition

Proximate, elemental/isotopic, and pigment analyses were used to evaluate the physiological state of kelp recovered from B-E and PL, and to assess nutrient uptake in depth-cycled kelp. Stable carbon (C) and nitrogen (N) isotope composition of kelp was used to explore whether depth-cycled kelp exhibited a distinct isotopic signature reflecting nitrogen uptake at deeper depths.

For proximate analysis, air dried blade tissue was pooled into ~50 g samples (2 per site) and shipped to Eurofins DCQI LLC for analysis using the following AOAC International standard methods: Protein-Combustion AOAC 990.03; AOAC 992.15, Ash-Combustion AOAC 942.05, Fat-Acid Hydrolysis AOAC 954.02, Carbohydrates-Calculated CFR 21-calc.

For elemental-isotopic analysis, dried blade tissue was powdered using a mortar and pestle, and approximately 1.8 mg was analyzed (in triplicates for each sample and six biological replicates per site). Elemental (% N and % C) and stable isotopic composition ($\delta^{15}N$ and

$\delta^{13}C$) were determined by continuous-flow isotope ratio mass spectrometry (CF-IRMS) using a Costech ECS 4010 elemental analyzer interfaced to a Micromass Isoprime mass spectrometer. Technical replicates were averaged to obtain values for each biological replicate.

Pigment content of frozen tissue was analyzed using the methods described in Campbell et al. [40]. Briefly, pigment was extracted in DMSO followed by methanol, and pigment concentrations measured via spectrophotometry using equations from Seely et al. [41] and Ritchie [42].

2.6. Statistical analysis

Daily average temperatures and daily average estimated nitrate concentrations were compared using a Kruskal-Wallis Test with Bonferroni correction applied to pairwise comparisons of each site. Differences in stipe elongation rate (cm day^{-1} and % per day), pneumatocyst wall thickness, blade length, blade width, wet-dry weight ratio, pigment concentrations, C and N content, and isotope ratios between sites were compared using Welch's unequal variance T-test. Data for recovered wet weight, % weight increase per day, number of stipes greater than 1-m in length, number of fronds upon recovery, pneumatocyst width, and blade-stem length failed the Shapiro-Wilk test of normality and were thus compared using the Mann-Whitney Rank Sum Test. Proximate analysis results (% Ash, % Protein, % Carbohydrates, % Crude Fat) were compared using a pooled-variance T-test to increase statistical power as a two-tailed F test showed that σ_1 is considered equal to σ_2 ($p = 0.834$). All tests were carried out at a 95% level of confidence. A principal component analysis (PCA) of results from the elemental/isotopic composition analysis was obtained using the R statistical package.

3. Results and discussion

3.1. Environmental conditions

Ocean waters are frequently stratified, with surface waters containing low concentrations (<1 μM) of the dissolved inorganic nutrients nitrate and phosphate, and increasing concentrations below the thermocline reaching ~40 μM nitrate and ~4 μM phosphate in abyssal environments [43]. Such oligotrophic surface conditions present challenges for mariculture efforts, which the current study addressed by testing the biological effects of a novel depth-cycling approach. Consistent with oligotrophic surface conditions, surface nutrients were low at the B-E site, with nitrate and phosphate concentrations below 1 μM in seawater sampled from 10 m during three separate cruises (Fig. 3B, Table 1). In contrast, seawater sampled from 70 m at the B-E site contained >15 μM nitrate and >1.5 μM phosphate. Temperature logs on the B-E clearly reflect successful depth-cycling between the nutrient deficient surface and nutritionally replete deeper environment, with rapid changes of 3–10 °C accompanying each transition between the deep and shallow positions (Fig. S3). Nutrient concentrations throughout the water column were tightly coupled to vertical temperature gradients, as evident by the temperature-depth profiles during all three cruises (Fig. 4). These profiles confirmed that the daytime kelp position was either at the Mixed Layer Depth (MLD) or above both the MLD and thermocline during all three cruises (Fig. 4A). At the surface position, kelp were exposed to warmer temperatures that increased from ~17 °C to ~21 °C over the course of the experiment (Fig. 5A, Tables S4 and S5). In contrast, the nighttime kelp position at ~80 m exhibited a relatively constant temperature of ~10 °C (Fig. 5A, Table S4) and was consistently below the thermocline (Fig. 4A).

Conditions at the other study sites were typical for nearshore waters at Catalina Island during mild El Nino conditions (https://psl.noaa.gov/enso/mei/index.html). Temperatures at BFC and PL ranged between 12 °C and 22 °C (Fig. S3). Similar to the surface position at the B-E site, daily averaged temperatures increased at both BFC and PL between May and September (Fig. 5A, Table S4) with high short-term variability (hourly fluctuations of 3 °C or more; Fig. S3), likely reflecting internal waves as observed by Zimmerman and Kremer [44]. Nitrate concentrations in water samples from these sites were between 0 and 5 μM (Table 1). Levels of nitrite and ammonia were found to be negligible at all sites and depths.

Nitrogen is generally considered to be one of the key factors limiting growth of giant kelp in Southern California [44–46]. To determine overall nitrate availability at each site, we relied on the close inverse correlation between seawater temperature and nitrate concentration in coastal upwelling regions such as the SCB [34,47,48] which enables predictions of nitrate concentration using temperature data. Building on these observations, *in-situ* temperature and nitrate concentrations from

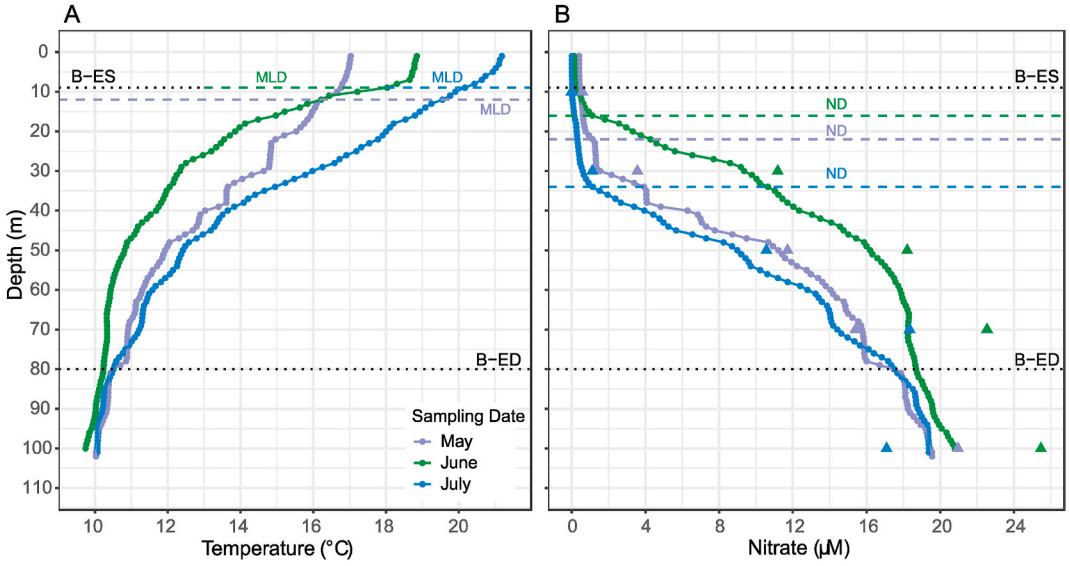

Fig. 4. Temperature, estimated nitrate, and measured nitrate profiles at the B-E site. Dotted reference lines represent the kelp surface position (B-ES) at ~9 m and deep position (B-ED) at ~80 m. (A) Temperature-depth profiles collected on three dates: 9/5/2019 (purple), 6/18/2019 (green), and 7/24/2019 (blue). Dashed reference lines represent the MLD. (B) Nitrate measurements and estimated nitrate-depth profiles. Nitrate measurements at 10, 30, 50, 70 and 100 m on the same three dates (triangles) and estimated nitrate concentrations (circles) at 1 m resolution predicted from the temperature-nitrate GAM using discrete temperature measurements from panel (A). Nutricline depths (ND) indicate estimated nitrate concentrations of 1.025 μM.

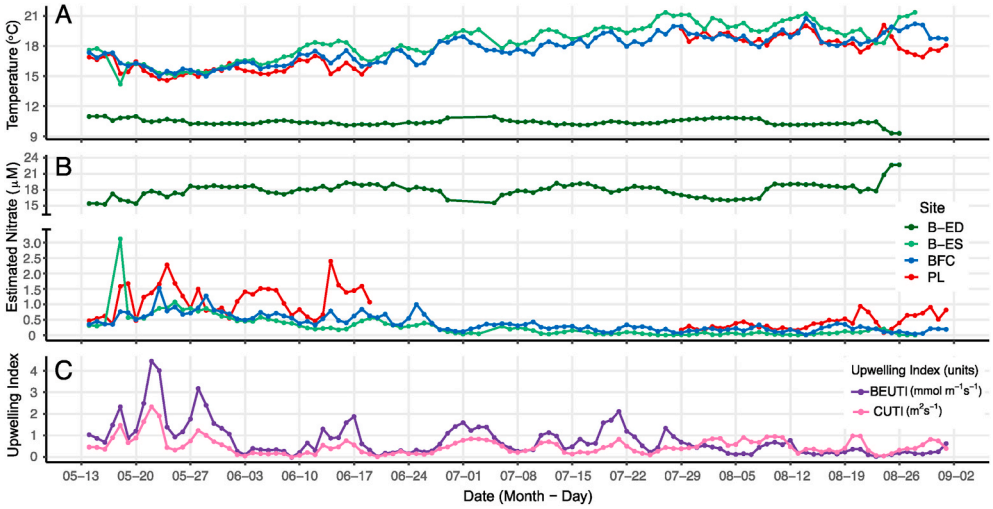

Fig. 5. Daily average temperatures, estimated nitrate concentrations, and upwelling indices during the experiment. (A) Continuously measured temperature (°C) data averaged daily for the three experimental sites: 1) B-E (B-ED: Deep, B-ES: Surface), 2) BFC, and 3) PL. (B) Daily average GAM estimated nitrate (μM) concentrations computed from continuously collected temperature data. (C) Two different upwelling indices for 33°N along the U.S. west coast: 1) BEUTI (mmol m^{-1} s^{-1}) and 2) CUTI (m^2 s^{-1}). The date range for all figures (x-axis) begins on 5/13/2019 and ends 2/9/2019.

CTD and water sampling casts during the experiment and within a prior 2-year period (Fig. S2, Tables S1 and S2) were used to determine the temperature-nitrate relationship at our study site (Fig. 6). While linear regression models have previously been used to derive temperature-nitrate relationships, GAM provides a better prediction of these relationships [34]. A similar GAM to the one used by Snyder et al. [34] was fit to this temperature and nitrate dataset. Although Snyder et al. [34] used a much more robust dataset (n > 2600), the GAM from this study, with an $R^2 = 0.957$; $p < 0.001$; $n = 85$, produced a very similar fit.

Using data from high frequency temperature loggers installed at or near the sites and our temperature-nitrate model, we then calculated estimated ambient nitrate concentrations. (Fig. 5B). Partitioning the temperature data between deep and surface positions at the B-E (Fig. 5B, Tables S6 and S7) shows that the nitrate exposure in the deep position on the B-E greatly exceeded nitrate exposure at PL or BFC. Depth-cycled kelp experienced an average nitrate concentration >15 μM in the deep position, which is both higher than what is typical for *Macrocystis* on Catalina Island [44] and has been shown to saturate growth in both field and laboratory studies [44,46,49]. In contrast, the B-E shallow position experienced nitrate concentrations <1 μM for most of the experiment,

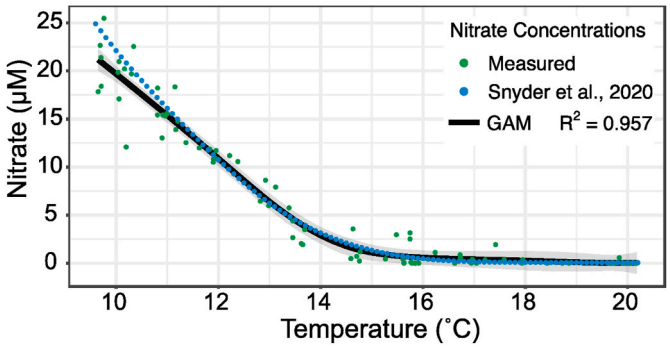

Fig. 6. Temperature-nitrate relationship model. Corresponding temperature and nitrate data for 85 seawater samples collected between 11/1/2017 and 7/25/2019 at the B-E, PL, BFC, and surrounding waters from multiple depths. Formula: nitrate ~ s(temperature, k = 10); parametric coefficients: intercept estimate = 6.49, std. error = 0.1737, t-value = 37.38, Pr (>|t|) = $<2e^{-16}$; approximate significant of smooth terms: s(temperature) estimated d.f. = 5.21, F = 295.1, $p < 2e^{-16}$. GAM fit for temperature to nitrate relationship (R^2 = 0.957, $p < 0.001$) is represented by the black line with the gray bars representing the standard error about the curve. Measured nitrate concentrations (μM) are in green while estimated nitrate (μM) from the summer GAM constructed by Snyder et al., 2020 is in blue.

though it is possible that the daily vertical movements of the B-E structure facilitated some deep-water mixing at the surface.

Daily average predicted nitrate exposure at PL was < 4 μM (Fig. 5B, Table S6). Periodic decreases in temperature and corresponding increases in nitrate exposure correlate well with the BEUTI and CUTI upwelling indices (Fig. 5B and C). Overall temperature trends at BFC and PL were similar (Fig. 5A, Tables S4 and S5), but temperature at BFC rarely dropped below the 14 °C threshold where nitrate concentrations increase with decreasing temperatures (Fig. S3) suggesting N limitations at this location (Fig. 5B, Tables S6 and S7).

3.2. Growth and morphology

To our knowledge, this is the first experiment to test the growth of kelp under depth-cycling conditions. The growth of depth-cycled kelp exceeded that of kelp transplanted to a fixed depth on the benthos or suspended in the water column at PL and BFC, respectively (Figs. 7–9). Kelp on the B-E initially declined in length, presumably a result of tissue removed during a storm just after deployment. Net growth resumed by June 10 (day 27) (Fig. 8), and by day 41 the majority of individuals were between 50 and 120 cm in length. An average length increase of 2.2 cm day^{-1} over the 18 day period between May 23 (day 9) and June 10 (day 27) is comparable to previously documented daily length increases for juvenile *Macrocystis* of 1.0–2.5 cm day^{-1} [22,50,51], suggesting growth was not negatively impacted by depth-cycling.

Over the entire course of the experiment the wet weight of kelp transplanted to B-E increased at an average overall rate of 5% per day resulting in a final wet weight ~4 times greater than kelp at PL, the site of a naturally occurring kelp bed (Fig. 9). This is despite almost all of the longest fronds on depth-cycled kelp being severed, presumably due to the failure of the B-E cable near the end of the experiment (see Methods). The heaviest B-E individual had a wet weight of 5.76 kg (Fig. 7J), and the longest individual stipe measured 6.3 m. At PL, the heaviest individual was 1.6 kg (Fig. 7G), and the longest stipe was 2.6 m. These maximum values indicate the potential yield of individual kelp which possibly could be expanded to mariculture operations using selection strategies and germplasm resources [16]. Juveniles transplanted to BFC did not survive (Fig. 7), possibly due to nutrient limitation (Fig. 5B), though other factors such as herbivory, limited water flow, and thermal stress cannot be ruled out [52].

Overall development also proceeded more rapidly at B-E. Standardized elongation rates for fronds that were not severed at B-E (mean RER = 3.27% per day, Stdev = 0.86, n = 12) were greater (d.f. = 21.0, T = 4.85, $p < 0.001$) than at PL (mean RER = 1.85% per day, Stdev = 0.85, n = 29) over the last half of the experiment and over three times greater

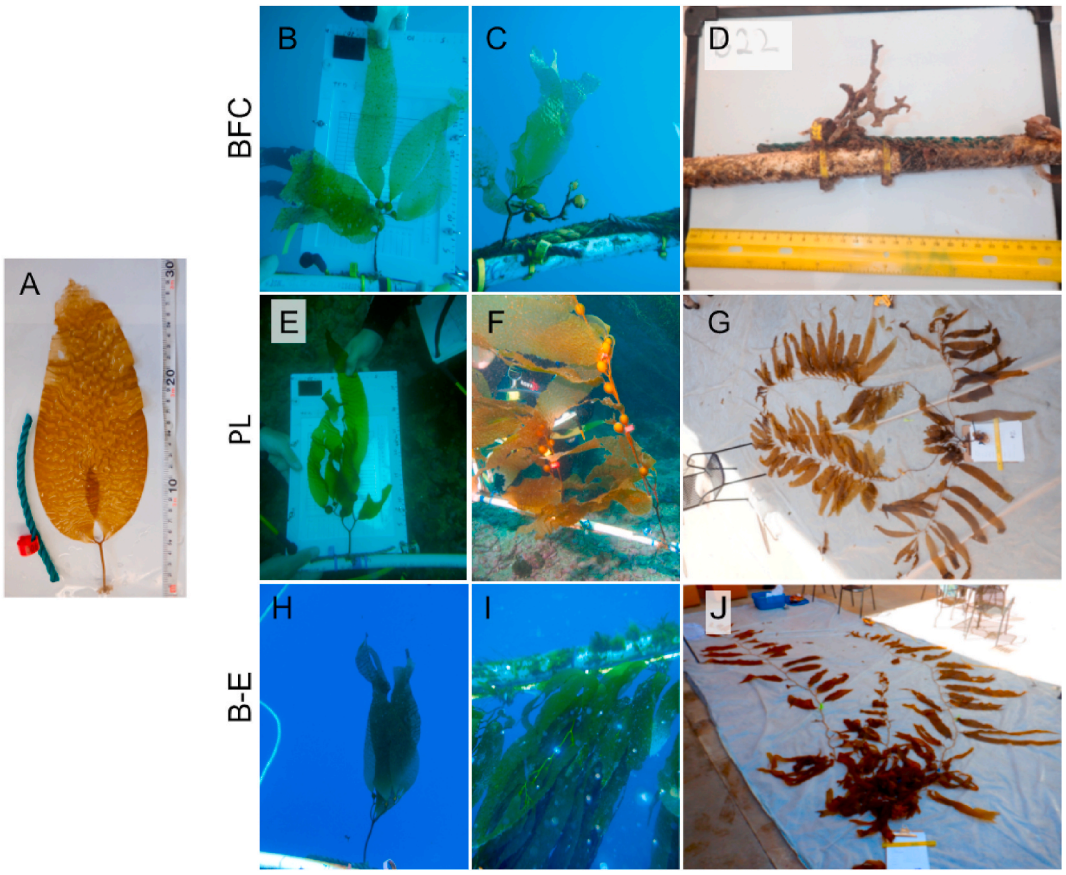

Fig. 7. Images of representative kelp during the experiment. (A) Juvenile kelp before deployment. (B–D) Kelp grown at BFC on days 27 (B), 65 (C), and 119 (D) post-deployment. (E–G) Kelp grown at PL on days 27 (E), 65 (F) and 113 (G) post-deployment. (H–I) Kelp grown at B-E on days 27 (H), 62 (I) and 107 (J) post-deployment. The individuals with the most wet biomass recovered from PL (1.6 kg) and B-E (5.76 kg) are shown in (G) and (J), respectively.

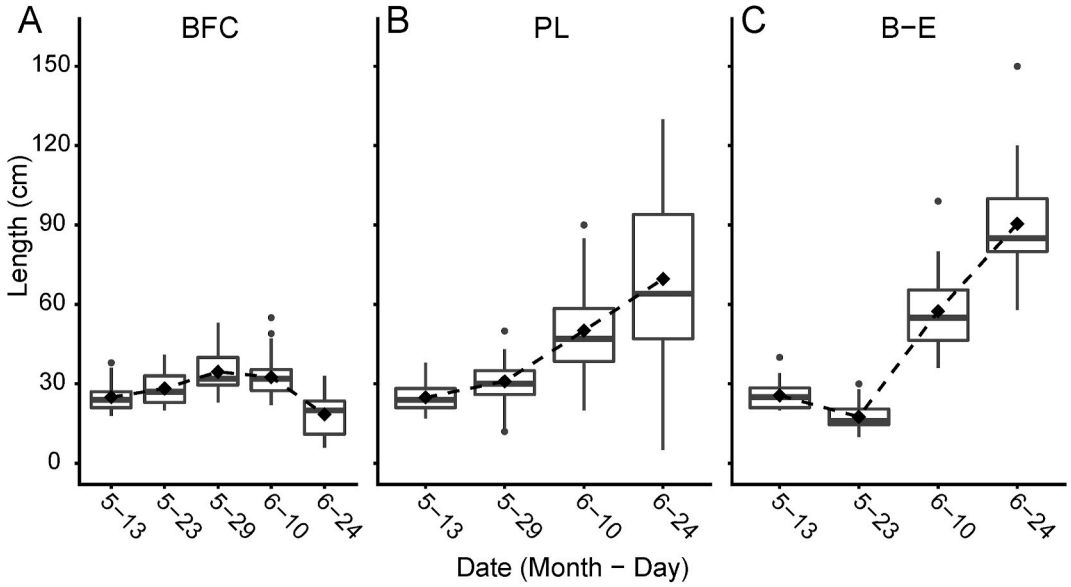

Fig. 8. *In-situ* length measurements of juvenile kelp. Lengths from holdfast to furthest blade tip for individuals at BFC (A, n = 35), PL (B, n = 35), and the B-E (C, n = 28) between 5/13/2019 (t = 0 days) and 6/24/2019 (t = 42 days).

on a centimeter per day basis (Fig. 10A). Furthermore, a census of fronds showed that by August 12 (day 90) most individuals (90%) on the B-E had at least 2 fronds greater than 1 m in length, while at PL on August 8 (day 86) the majority of kelp (74%) had no fronds achieving this length (Fig. 10B). Frond initiation rates were also greater; kelp recovered from B-E (n = 30) at the end of the experiment had an average of seven fronds or developing apical meristems compared to four at PL (n = 26) ($U = 704.5$, $Z = 5.30$, $P < 0.001$). In summary, daily cycling between ~9 and

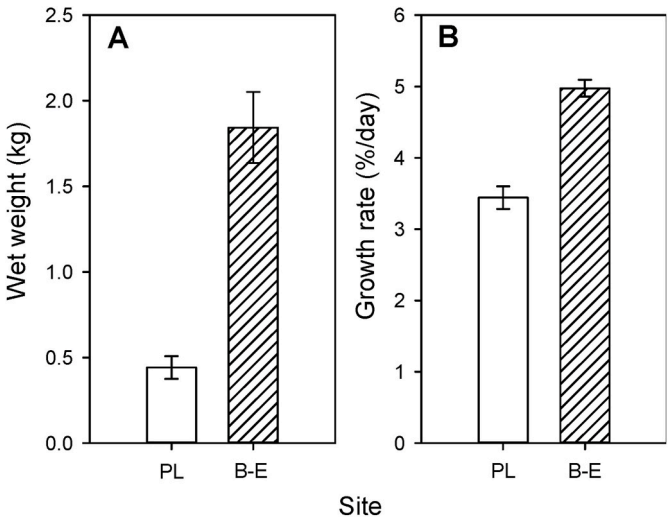

Fig. 9. Recovered wet weights and growth rate from B-E (n = 30) and PL (n = 27). (A) Average wet weight for all kelp recovered. Wet weights are plotted with standard error bars (U = 756.0, Z = 5.60 p < 0.001). (B) Average percent increase in wet weight per day at PL and B-E plotted with standard error bars (U = 759.0, Z = 5.65, p < 0.001).

~80 m of depth appeared to have no negative effects on giant kelp, and in fact significantly enhanced growth relative to individuals transplanted back to the kelp bed from which the juvenile kelp were originally obtained.

Macrocystis is known to have a large degree of morphological plasticity in response to environmental conditions (e.g. Ref. [53]), so the effect of depth-cycling on morphology was investigated. Of particular interest was whether pneumatocyst development would be affected by exposure to high pressures at depth. Previous work [22] found that pneumatocysts formed at shallow depths ruptured when *Macrocystis* was transplanted to deeper water, but that kelp grown from a pre-pneumatocyst stage in deep water were able to form pneumatocysts that did not rupture. During in-water observations and upon harvest we found that the majority of pneumatocysts on the depth-cycled kelp appeared undamaged but had morphologies distinct from those found at PL where pneumatocysts closely resembled that of nearby undisturbed individuals. Pneumatocysts of depth-cycled kelp were significantly narrower and had a greater range of blade stem lengths (Width: U = 728.0, Z = 6.33, p < 0.001; Blade stem length: U = 0.0, Z = −6.29, p < 0.001, Fig. 11). Pneumatocyst walls were also significantly thicker (d.f. = 34.48, T = −10.45, p < 0.001, Fig. 11). A surprising finding was that each of the depth-cycled pneumatocysts sliced open for measurement was fluid-filled, with at most a small gas bubble present within the fluid. Since aqueous fluids are incompressible this likely explains the absence of ruptured bladders. Moreover, we found no evidence that the outer layer of the depth-cycled pneumatocysts were compromised, suggesting that the fluid accumulated internally. During the experiment, kelp at the B-E appeared to have slight negative buoyancy consistent with the absence of gas in pneumatocysts causing fronds to stream out in the current rather than float towards the surface. The presence of fluid was in contrast to pneumatocysts from PL, which were filled with gas as is typical for *Macrocystis*. The change in expected buoyancy of bladder kelp requires further investigation to inform future farm designs that will need to take into account how this parameter could impact biological requirements (e.g., light availability) and engineering constraints (e.g., drag).

Other morphological differences between depth-cycled individuals and those outplanted to PL include longer and wider blades (Fig. 12), as well as the possible presence of sorus tissue on basal blades of depth-cycled kelp. The latter observation is based on qualitative assessments of blades that appeared to contain darkened patches characteristic of sorus tissue (Fig. 13), but the presence and viability of spores could not be tested. Darkened patches were not noticeably present on kelp at PL.

It is unclear which environmental differences between the PL kelp bed and B-E site were responsible for these morphological differences. As previously described depth-cycled kelp experienced substantial pressure changes and daily exposure to cold nutrient-rich water, but other unmeasured variables such as differences in water motion (which can increase rates of both nutrient uptake and photosynthesis [54]), biotic interactions with other species (e.g., herbivorous fish and invertebrate species typical of PL but not B-E) and thermoregulatory

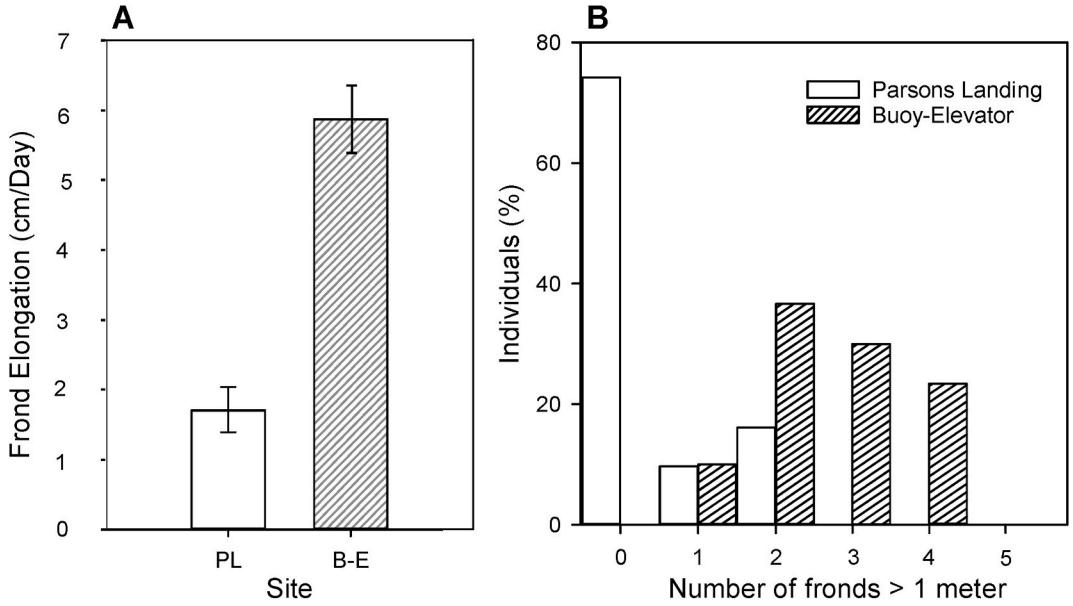

Fig. 10. Frond elongation rates and *in-situ* frond measurements. (A) Elongation rates of intact fronds at harvest from B-E (n = 12 previously tagged fronds) and PL (n = 29 previously tagged fronds) plotted with error bars showing standard error (d.f. = 12.7, T = 5.36, p < 0.001). (B) Survey of fronds longer than 1 m per individual at PL (8/8/2019, n = 30) and B-E (8/12/2019, n = 29). Average number of fronds greater than 1 m was 0.42 fronds at PL and 2.67 at B-E (U = 883.0, Z = 6.27, p < 0.001).

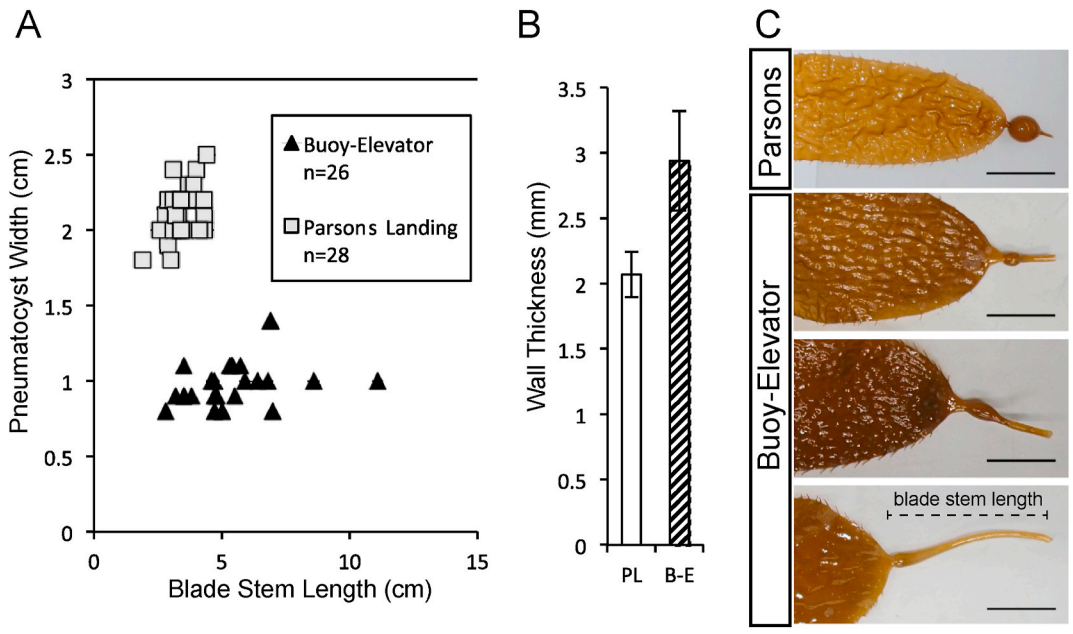

Fig. 11. Pneumatocyst morphology. (A) Blade stem length (measured from the end of the pneumatocyst to the stipe) and pneumatocyst width for samples from both sites. Average width is 0.98 cm (Stdev = 0.13) at B-E and 2.12 cm (Stdev = 0.17) at PL. Average length is 5.31 cm (Stdev = 1.78) at B-E and 3.44 cm (Stdev = 0.59) at PL. (B) Wall thickness of pneumatocysts from PL (n = 28) and the B-E (n = 26), with error bars showing standard deviation. (C) Representative pneumatocysts from PL (top) and the B-E (bottom three), scale bar is 5 cm.

Fig. 12. Patches resembling sorus tissue on blades from the B-E site.

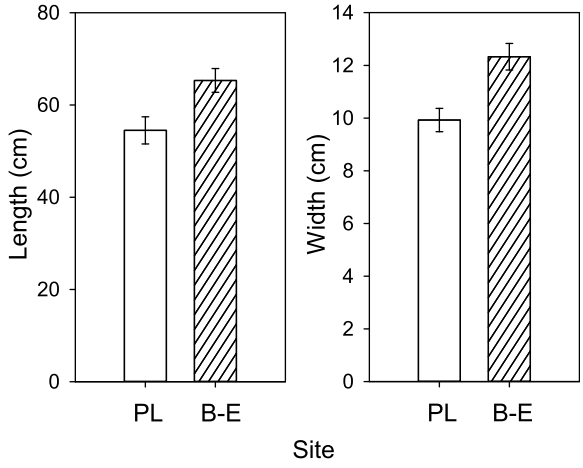

Fig. 13. Blade Morphology. Length (left) and width (right) of randomly sampled kelp blades from the B-E (n = 43) and Parsons Landing (PL, n = 19) at the end of the experiment. Average blade length and width were significantly greater at B-E than PL (d.f. = 44.86, T = 2.76, p = 0.008 and d.f. = 55.03, T = 3.59, p < 0.001, respectively).

metabolic responses may have also affected morphological development and reproductive capacity. Work on natural populations of *Macrocystis* suggests that sorus production can be stimulated by increased nitrogen exposure [55], though observations of small individuals with mature sorus in the upper sublittoral fringe [56] and four months after recruitment in the rocky intertidal [51] suggest that additional environmental factors such as water motion could also influence precocious sorus formation. Similarly, Stephens and Hepburn [57] observed that exposure to pulses of increased nitrate concentrations increased blade thickness and reduced erosion rates suggesting that the repeated exposure to saturating levels of nitrate via depth-cycling in this study may explain some of the differences in blade size. Another possibility is that water motion differences affected blade morphology, as differences in blade shape between individuals growing in high versus low wave energy environments are also well documented [58].

3.3. Tissue composition

Growth rates for depth-cycled kelp exceeded those of kelp transplanted to a fixed depth on a reef where they naturally occur, and relative differences in average nitrate availability at each site correlate with differences in kelp growth (Figs. 5 and 7). This suggests that depth-cycled kelp may have been less nitrogen limited than kelp at other sites.

Recent work investigating the growth response of *Macrocystis* to simulated *in-situ* pulses of nitrate (via potassium nitrate dissolution blocks) found that during N deficient periods, N fertilization did not enhance frond elongation rates but instead promoted tissue maintenance [57]. Similarly, it is possible that pulses of nitrate supplied by episodic upwelling or internal waves (Fig. 5B and C) at PL may have been sufficient to support tissue maintenance but might not have been enough to promote high growth rates.

While the rapid growth of depth-cycled kelp suggests successful uptake of N from deep water, previous work has found that both depth (0 m vs 12 m) and an absence of light may impede the uptake of nitrate by *Macrocystis* [46]. In contrast, recent transcriptomic work assessing gene expression of vegetative blades along a frond sampled at the surface (0 m) and near the holdfast (18 m) found a higher level of N assimilation (e.g. nitrite/nitrate reductase) gene expression in deeper water [59]. Although these different studies support some degree of N uptake at depth, a major concern was whether deeper depths (in this case ~80 m) combined with a complete absence of light might prevent N uptake entirely. To support the idea that the increased growth of depth-cycled kelp reflected successful uptake of nitrate during the deep phase of each cycle, we analyzed key parameters related to N assimilation in tissue recovered from B-E and PL (Tables 2–4).

Proximate analysis of pooled blade tissue from the B-E and PL kelp showed that kelp grown at B-E had nearly twice the protein content and significantly lower ash content compared to kelp transplanted to PL (Table 2). A previous study of Southern and Central California *Macrocystis* found protein ranged from 5 to 14% of total dry mass ([60] via [61]). Blades recovered from depth-cycled kelp were ~12% protein, indicating that depth-cycling did not significantly impede N assimilation. Pigment concentration measurements showed lower chlorophyll-*a* content (on a dry-weight basis) and a higher molar ratio of chlorophyll-*c*:chlorophyll-*a* at B-E compared to PL (Table 3). Differences in pigment concentrations and ratios were likely caused by interactive effects between light and nutrient availability at each site [62].

Elemental analysis of C and N further supports the conclusion that depth-cycling did not impede N assimilation, with kelp from B-E having a lower C:N ratio and significantly higher N content (% dry weight, mean % N of 1.9) than kelp from PL (Table 4, Fig. 13). Interestingly, depth-cycled kelp from this study exhibited even lower C:N and higher N content than kelp tissue from N fertilization experiments [57] and *Macrocystis* exhibiting enhanced growth at wave-exposed sites [63]. Laboratory studies using juvenile sporophytes [49] showed that specific growth rates increased rapidly as N content increases to 1% but leveled off thereafter. Similar results were obtained by Gerard [64] who found that growth rates for a mature sporophyte transplanted to nitrate-deficient waters were maintained until internal N declined to ~1% at which point growth sharply declined. Taken together, the tissue composition of kelp recovered from B-E suggest that growth was not N limited.

To explore the possibility that N and C assimilated by depth-cycled kelp would have a unique isotopic signature, tissue $\delta^{15}N$ and $\delta^{13}C$ were analyzed. Blades from B-E had a significantly higher $\delta^{15}N$ value than PL (Table 4). The dissolved subsurface nitrate in the SCB, including two stations sampled in the San Pedro Basin close to the B-E site, are reported to have a mean $\delta^{15}N$ signature of 9 ± 0.7‰ with a $\delta^{15}N$ maximum of ~11.5‰ at 350 m [65]. More recent work has also shown that $\delta^{15}N$ increases with depth along the Southern/Baja California coast at depths above 300 m, with a weaker signature near Point Conception that becomes stronger further south [66]. A higher $\delta^{15}N$ signature in depth-cycled kelp most likely indicates that the N accumulated in depth-cycled kelp tissue had a deeper origin than the N incorporated at PL. Foley and Koch [67] also report a difference in $\delta^{15}N$ values between kelp sampled along central California at 5 m and 15 m during late summer and fall, where even a difference of 10 m resulted in the deeper kelp tissue exhibiting higher $\delta^{15}N$ values. As previously described, ambient nitrate at the B-E surface position was extremely limited (Fig. 5B), thus the accumulation of N and nitrogenous compounds in depth-cycled kelp coupled with a heavier $\delta^{15}N$ signature strongly supports the conclusion that *Macrocystis* was able to absorb and utilize N obtained at depth and in the absence of light.

Interestingly, depth-cycled kelp also had a significantly higher $\delta^{13}C$ compared to PL (Table 4). Elevated $\delta^{13}C$ is often a consequence of CO_2 depletion at the blade surface at high photosynthetic rates [68]. Because C fixation would have occurred during daylight hours when kelp from both B-E and PL were at a similar depth (~9 m) and presumably exposed to isotopically similar pools of dissolved inorganic carbon, the higher $\delta^{13}C$ signature associated with B-E kelp might reflect more rapid assimilation of C. The higher growth rates (Figs. 9 and 10) and greater %

Table 3
Percent dry weight, tissue pigment concentrations (mg g^{-1} dw), and pigment molar ratios of blades recovered from PL and B-E.

Measurement		PL n = 6	B-E n = 6	d.f	t-statistic	p-value
% Dry Weight	Mean	12.07	15.53	8.27	4.24	0.0026
	Stdev	0.010	1.705			
Chlorophyll-*a*	Mean	1.90	1.60	8.41	−3.78	0.0049
	Stdev	0.165	0.104			
Chlorophyll-*c*	Mean	0.67	0.93	8.85	2.24	0.0523
	Stdev	0.232	0.159			
Fucoxanthin	Mean	0.29	0.30	6.19	0.17	0.8677
	Stdev	0.123	0.043			
Chl-*c*: Chl-*a*	Mean	0.51	0.85	9.87	4.09	0.0022
	Stdev	0.150	0.134			
Fuco: Chl-*a*	Mean	0.20	0.25	6.27	1.58	0.1626
	Stdev	0.074	0.027			

Table 4
Elemental analysis of blade tissue at the end of the experiment. % C and % N are percentage dry weight.

Value		PL n = 6	B-E n = 6	d.f.	t-statistic	p-value
% C	Mean	25.36	28.72	9.43	−3.70	0.0045
	Stdev	1.76	1.37			
% N	Mean	1.04	1.89	9.26	−3.35	0.00825
	Stdev	0.37	0.50			
C:N	Mean	27.27	15.98	6.34	2.56	0.04087
	Stdev	10.12	3.74			
$\delta^{15}N$	Mean	7.06	10.21	9.28	−3.54	0.00538
	Stdev	1.51	1.57			
$\delta^{13}C$	Mean	−17.14	−11.78	8.93	−5.28	0.000522
	Stdev	1.42	2.04			

Table 2
Proximate analysis results of combined kelp tissue from the B-E and PL at the end of the experiment (two replicates from each site).

		Ash (%)	Carbohydrates (%)	Crude Fat (%)	Protein (%)
B-E	Rep-1	41.42	44.97	1.38	12.23
	Rep-2	42.18	43.69	1.47	12.66
PL	Rep-1	46.35	44.96	1.26	7.43
	Rep-2	48.92	42.96	1.36	6.87
	d.f.	2.0	2.0	2.0	2.0
	t-statistic	−4.35	0.31	1.71	15.0
	p-value	0.049	0.785	0.229	0.004

C (Table 4) observed for depth-cycled kelp further support the potential for higher photosynthetic rates at the B-E site relative to PL. Interestingly, Foley and Koch [67] also note a distinct difference between $\delta^{13}C$ values of kelp collected at 5 and 15 m depth during an upwelling period, with the surface blades exhibiting higher $\delta^{13}C$ values potentially due to increased draw down of CO_2. A further possible explanation can be found from studies of C isotope fractionation in phytoplankton. While the fractionation dynamics of C isotopes in marine primary producers is complex, in diatoms it appears that N limited growth is associated with an increase in fractionation as compared to light limited growth [69]. Similarly, greater N availability due to depth-cycling at the B-E site (Fig. 5B), reflected in higher N and protein content, seems to support greater C fixation resulting in higher C content, lower C:N, and heavier $\delta^{13}C$ values for depth-cycled kelp as compared to PL (Fig. 14, Table 5).

Together, these results suggest that ambient nitrogen accumulated during the deep phase of each depth-cycle supported kelp growth, which exceeded that of kelp at PL and BFC where nitrogen was more limited, although we cannot rule out the possibility that other untested environmental factors such as water motion, light availability, or herbivory contributed to these differences.

3.4. Conclusions

Results from this study provide the first documentation of growth and development of *Macrocystis pyrifera* under daily depth-cycling conditions, demonstrating that this species is compatible with a depth-cycling cultivation strategy. Extensive efforts during the Marine Biomass Program of the 1970's and 1980's [9] provide a framework for investigating macroalgae as a bio-fuel feedstock, and here we add an alternative to previously described artificial upwelling strategies. Though previous work has shown that both the absence of light and an increase in depth may negatively impact the ability of *Macrocystis* to assimilate nitrate [46], the results from this study show that any such reduction in uptake rate is compensated by frequent exposure to saturating nitrate concentrations below the thermocline.

Depth-cycling may also provide a mechanism to prevent thermal stress both through the avoidance of excessively warm surface conditions and by increasing nitrate availability [70], an important consideration in the context of global warming and climatic regimes such as El Niño events. This is consistent with work by Clendenning and Sargent [71] who found that the highest photosynthetic rates for Southern California *Macrocystis* were between 20° and 25 °C and that 25–30 °C was optimal for Baja California kelp. These results suggest that *Macrocystis* supplied with sufficient nutrients via depth-cycling could tolerate relatively warm surface conditions, especially if consideration were given to cultivation of warm-water adapted genotypes.

Engineering studies for depth-cycling open ocean farms are currently underway (Fig. S4), and the impact of altered pneumatocyst buoyancy will have to be accounted for in these designs. Additional depth-cycling trials are also required to understand the growth and development of more mature kelp, particularly when the kelp reach harvest size. The frequency and duration of depth-cycling as well as selection of depths should also be considered in the context of uptake kinetics and nutrient storage to potentially enhance biomass yields [72]. Logistical costs and technological developments aside, this study suggests that *Macrocystis* can be grown under depth-cycling conditions, and that this technique may offer a viable approach to circumventing surface nutrient limitations facilitating large-scale and year-round production of macroalgae as feedstock for low-carbon fuels.

Author contributions

IA Navarrete: Methodology, Investigation, Formal analysis, Writing – original draft, Visualization. DY Kim: Conceptualization, Methodology, Supervision, Investigation, Formal analysis, Writing – review & editing. C Wilcox: Conceptualization, Project administration, Funding acquisition. DC Reed: Conceptualization, Methodology. DW Ginsburg: Conceptualization, Methodology, Supervision, Investigation, Visualization. JM Dutton: Conceptualization, Resources. J Heidelberg: Project administration, Supervision, Resources. Y Raut: Formal analysis, Visualization. BH Wilcox: Conceptualization, Methodology, Funding acquisition, Resources.

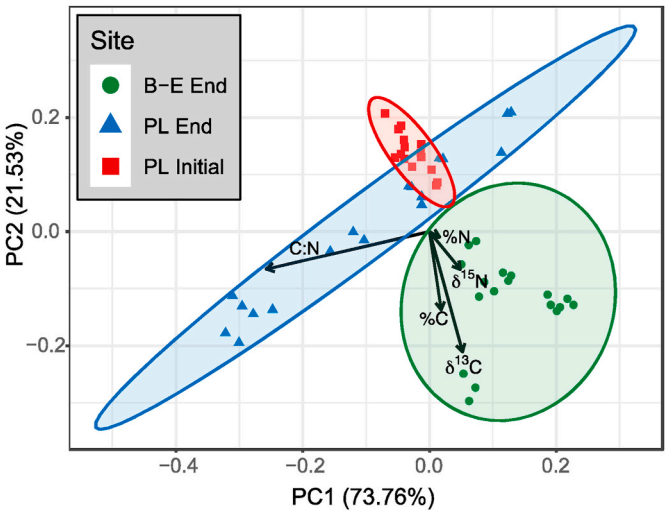

Fig. 14. Principal component analysis of elemental and isotopic C and N content. Plot based on the first 2 principal components of kelp tissue composition using % C, % N, C:N, $\delta^{15}N$, and $\delta^{13}C$ values from samples collected initially at PL (red) and at the end of the experiment from both PL (blue) and B-E (green) sites. The 95% confidence ellipses are shaded corresponding to the different samples.

Table 5
Elemental analysis PCA results. The bold values represent the highly significant (>|0.5|) factor loadings of the variables for each PCA axes.

	Factor Loadings				
Variables	PC1	PC2	PC3	PC4	PC5
% C	0.0688	**−0.511**	−0.238	**0.821**	0.0544
% N	0.0596	−0.0359	−0.0425	0.0264	**−0.996**
C:N ratio	**−0.959**	−0.245	0.124	−0.0329	−0.0547
$\delta^{15}N$	0.182	−0.247	**0.946**	0.106	−0.0178
$\delta^{13}C$	0.195	**−0.785**	−0.180	−0.559	0.0328
Eigenvalues	62.48	18.24	3.340	0.614	0.030
Standard deviation	7.904	4.271	1.828	0.784	0.174
Proportion of Variance	0.738	0.215	0.0394	0.00725	0.00036
Cumulative Proportion	0.738	0.953	0.992	0.9996	1

Declaration of competing interest

Brian Wilcox and Cindy Wilcox declare that they own the relevant intellectual property and majority shares in Marine BioEnergy, Inc. Brian Wilcox and Cindy Wilcox declare that they have no personal relationships that could have appeared to influence the work reported in this paper. Diane Kim declares that she is co-founder of Holdfast Aquaculture, LLC and declares no competing financial interests or personal relationships that could have appeared to influence the work reported in this paper. The remaining authors declare that they have no known competing financial interests or personal relationships that could have appeared to influence the work reported in this paper.

Acknowledgements

The information, data, or work presented herein was funded in part

by the Advanced Research Projects Agency-Energy (ARPA-E), U.S. Department of Energy, under Award Number DE-AR0000689, United States.. The views and opinions of authors expressed herein do not necessarily state or reflect those of the United States Government or any agency thereof. All collections and transplanting activities were permitted under California Department of Fish and Wildlife Permit SC-13588. The buoy location and deployment permits were approved by the relevant federal, state, and local agencies. We would like to thank staff at the USC Wrigley Marine Science Center for supporting boat and dive operations for this project. Specifically, Eric Castillo, Lorraine Sadler, Ted Sharshan and Maurice Roper who provided their underwater expertise as research SCUBA divers; Gordon Bovin, Juan Aguilar, Trevor Oudin and Mariluz Fornias for their nautical leadership; Sean Conner, Lauren Czarnecki Oudin, Linda Duguay, Karen Erickson, Lauren Geving, Holly Nielson, Kellie Spafford and Victoria Sperow for onsite logistics and support; Karl Huggins for thoughtful discussions and access to the USC Hyperbaric Chamber; Troy Gunderson for his work on sampling cruises and processing CHN samples. Special thanks to Dr. Douglas Capone who provided access to his lab to run samples for CHN and isotope analysis. We also thank the Catalina Conservation Divers who provided temperature data for BFC. Finally, we would like to acknowledge all the undergraduate students who assisted us on various aspects of the project, especially Jacqueline Hernandez, Milena Castillo-Grynberg, James Sturges, Rilee Sanders, Tristan Jordan-Huffman, Sachi Elias, Emelly Ortiz, Andrea Munoz and Fotis Rimer, many of whom participated through either the USC Dornsife Environmental Studies Program or the NSF-sponsored USC Wrigley Institute Research Experiences for Undergraduates program (OCE- 1852220). The engineering group would like to thank John Leichty, Christopher McQuin, Jaret Matthews, Michael Hagman, Matthew Frost, Evan Schneider and Waymon Brown.

Appendix A. Supplementary data

Supplementary data to this article can be found online at https://doi.org/10.1016/j.rser.2021.110747.

References

[1] IPCC. Global Warming of 1.5°C. An IPCC Special Report on the impacts of global warming of 1.5°C above pre-industrial levels and related global greenhouse gas emission pathways. In: Global Warming of 1.5° C. An IPCC Special Report on the impacts of global warming of 1.5° C above pre-industrial levels and related global greenhouse gas emission pathways, in the context of strengthening the global response to the threat of climate change, sustainable development, and efforts to eradicate poverty. IPCC; 2018. https://www.ipcc.ch/site/assets/uploads/sites/2/2019/06/SR15_Full_Report_High_Res.pdf.

[2] Trisos CH, Merow C, Pigot AL. The projected timing of abrupt ecological disruption from climate change. Nature 2020;580:496–501. https://doi.org/10.1038/s41586-020-2189-9.

[3] van Dyk S, Su J, McMillan JD, Saddler JN. "Drop-in" Biofuels : the key role that co-processing will play in its production. IEA Bioenergy; 2019. https://www.ieabioenergy.com/wp-content/uploads/2019/09/Task-39-Drop-in-Biofuels-Full-Report-January-2019.pdf.

[4] FAO. The state of the world's land and water resources for food and agriculture-managing systems at risk. London: Food and Agriculture Organization of the United Nations, Rome and Earthscan; 2011. http://www.fao.org/3/i1688e/i1688e00.htm.

[5] Wei N, Quarterman J, Jin YS. Marine macroalgae: an untapped resource for producing fuels and chemicals. Trends Biotechnol 2013;31:70–7. https://doi.org/10.1016/j.tibtech.2012.10.009.

[6] Sudhakar K, Mamat R, Samykano M, Azmi WH, Ishak WFW, Yusaf T. An overview of marine macroalgae as bioresource. Renew Sustain Energy Rev 2018;91:165–79. https://doi.org/10.1016/j.rser.2018.03.100.

[7] Ross AB, Jones JM, Kubacki ML, Bridgeman T. Classification of macroalgae as fuel and its thermochemical behaviour. Bioresour Technol 2008;99:6494–504. https://doi.org/10.1016/j.biortech.2007.11.036.

[8] Wilcox HA. Prospects and problems in regard to farming the open oceans. In: 58th International Conference Alternative Energy and the Offer of the Sun and Sea, Milan, Italy. Palazzo CISI; 1980. p. 563–78.

[9] Bird KT, Benson PH, editors. Seaweed cultivation for renewable resources. New York: Elsevier; 1987.

[10] Van Der Molen J, Ruardij P, Mooney K, Kerrison P, O'Connor NE, Gorman E, et al. Modelling potential production of macroalgae farms in UK and Dutch coastal waters. Biogeosciences 2018;15:1123–47. https://doi.org/10.5194/bg-15-1123-2018.

[11] Song M, Duc Pham H, Seon J, Chul Woo H. Marine brown algae: a conundrum answer for sustainable biofuels production. Renew Sustain Energy Rev 2015;50:782–92. https://doi.org/10.1016/j.rser.2015.05.021.

[12] Roesijadi G, Jones SB, Snowden-Swan LJ, Zhu Y. Macroalgae as a biomass feedstock: a preliminary analysis (PNNL-19944). PNNL; 2010. https://www.pnnl.gov/main/publications/external/technical_reports/pnnl-19944.pdf.

[13] Stewart HL, Fram JP, Reed DC, Williams SL, Brzezinski MA, Maclntyreb S, et al. Differences in growth, morphology and tissue carbon and nitrogen of *Macrocystis pyrifera* within and at the outer edge of a giant kelp forest in California, USA. Mar Ecol Prog Ser 2009;375:101–12. https://doi.org/10.3354/meps07752.

[14] Rodriguez GE, Rassweiler A, Reed DC, Holbrook SJ. The importance of progressive senescence in the biomass dynamics of giant kelp (*Macrocystis pyrifera*). Ecology 2013;94:1848–58. https://doi.org/10.1890/12-1340.1.

[15] North WJ. Growth of individual fronds of the mature giant kelp, *Macrocystis*. In: North WJ, editor. The Biology of Giant Kelp Beds (Macrocystis) in California. Lehre, Germany: J. Cramer; 1971. p. 123–68.

[16] Wade R, Augyte S, Harden M, Nuzhdin S, Yarish C, Alberto F. Macroalgal germplasm banking for conservation, food security, and industry. PLoS Biol 2020;18:1–10. https://doi.org/10.1371/journal.pbio.3000641.

[17] Kim J, Stekoll M, Yarish C. Opportunities, challenges and future directions of open-water seaweed aquaculture in the United States. Phycologia 2019;58:446–61. https://doi.org/10.1080/00318884.2019.1625611.

[18] Graham MH, Vásquez JA, Buschmann AH. Global ecology of the giant kelp *Macrocystis*: from ecotypes to ecosystems. Oceanography and Marine Biology 2007;45:39–88. https://www.researchgate.net/publication/228620102_Global_ecology_of_the_giant_kelp_Macrocystis_From_ecotypes_to_ecosystems.

[19] Abdelrhman MA. Modeling water clarity and light quality in oceans. J Mar Sci Eng 2016;4. https://doi.org/10.3390/jmse4040080.

[20] Bristow LA, Mohr W, Ahmerkamp S, Kuypers MMM. Nutrients that limit growth in the ocean. Curr Biol 2017;27:R474–8. https://doi.org/10.1016/j.cub.2017.03.030.

[21] North WJ. Oceanic farming of *Macrocystis*, the problems and non-problems. In: Bird KT, Benson PH, editors. Seaweed Cultivation for Renewable Resources. New York: Elsevier; 1987. p. 39–67.

[22] Neushul M, Haxo FT. Studies on the giant kelp, *Macrocystis*. I. Growth of young plants. Am J Bot 1963;50:349. https://doi.org/10.2307/2440151.

[23] Harrison PJ, Hurd CL. Nutrient physiology of seaweeds: application of concepts to aquaculture. Cah Biol Mar 2001;42:71–82. https://doi.org/10.21411/CBM.A.D52FD22A.

[24] Haines KC, Wheeler PA. Ammonium and nitrate uptake by the marine macrophytes *Hypnea musvuformis* (Rhodophyta) and *Macrocystis pyrifera* (Phaeophyta). J Phycol 1978;14:319–24. https://doi.org/10.1111/j.1529-8817.1978.tb00305.x.

[25] Gordillo F, Dring M, Savidge G. Nitrate and phosphate uptake characteristics of three species of brown algae cultured at low salinity. Mar Ecol Prog Ser 2002;234:111–8. https://doi.org/10.3354/meps234111.

[26] Pereira R, Kraemer G, Yarish C, Sousa-Pinto I. Nitrogen uptake by gametophytes of *Porphyra dioica* (Bangiales, Rhodophyta) under controlled-culture conditions. Eur J Phycol 2008;43:107–18. https://doi.org/10.1080/09670260701763393.

[27] Harrison P, Parslow J, Conway H. Determination of nutrient uptake kinetic parameters: a comparison of methods. Mar Ecol Prog Ser 1989;52:301–12. https://doi.org/10.3354/meps052301.

[28] Raikar V, Wafar M. Surge ammonium uptake in macroalgae from a coral atoll. J Exp Mar Biol Ecol 2006;339:236–40. https://doi.org/10.1016/j.jembe.2006.08.002.

[29] Hickey BM. Circulation over the Santa Monica-San Pedro Basin and shelf. Prog Oceanogr 1992;30:37–115. https://doi.org/10.1016/0079-6611(92)90009-O.

[30] Berelson WM. The flushing of two deep-sea basins, southern California borderland. Limnol Oceanogr 1991;36:1150–66. https://doi.org/10.4319/lo.1991.36.6.1150.

[31] Bushing WW. Monitoring the persistence of giant kelp around Santa Catalina Island using a geographic information system. J Phycol 2000;36:9–10. https://doi.org/10.1046/j.1529-8817.1999.00001-27.x.

[32] Stewart HL, Carpenter RC. The effects of morphology and water flow on photosynthesis of marine macroalgae. Ecology 2003;84:2999–3012. https://doi.org/10.1890/02-0092.

[33] Fiedler PC. Comparison of objective descriptions of the thermocline. Limnol Oceanogr Methods 2010;8:313–25. https://doi.org/10.4319/lom.2010.8.313.

[34] Snyder JN, Bell TW, Siegel DA, Nidzieko NJ, Cavanaugh KC. Sea surface temperature imagery elucidates spatiotemporal nutrient patterns for offshore kelp aquaculture siting in the southern California Bight. Front Mar Sci 2020;7:1–14. https://doi.org/10.3389/fmars.2020.00022.

[35] Kara AB, Rochford PA, Hurlburt HE. An optimal definition for ocean mixed layer depth. J Geophys Res Ocean 2000;105:16803–21. https://doi.org/10.1029/2000jc900072.

[36] Richardson K, Bendtsen J. Vertical distribution of phytoplankton and primary production in relation to nutricline depth in the open ocean. Mar Ecol Prog Ser 2019;620:33–46. https://doi.org/10.3354/meps12960.

[37] Wood S. Generalized additive models: an introduction with R. 2 edition. Chapman and Hall/CRC; 2017.

[38] Jacox MG, Edwards CA, Hazen EL, Bograd SJ. Coastal upwelling revisited: ekman, bakun, and improved upwelling indices for the U.S. West coast. J Geophys Res Ocean 2018;123:7332–50. https://doi.org/10.1029/2018JC014187.

[39] NOAA. Southwest fisheries science center. 2020. https://oceanview.pfeg.noaa.gov/products/upwelling/dnld. [Accessed 20 May 2020].

[40] Campbell SJ, Bite JS, Burridge TR. Seasonal patterns in the photosynthetic capacity, tissue pigment and nutrient content of different developmental stages of

Undaria pinnatifida (phaeophyta: laminariales) in Port Phillip Bay, South-Eastern Australia. Bot Mar 1999;42:231–41. https://doi.org/10.1515/BOT.1999.027.
[41] Seely GR, Duncan MJ, Vidaver WE. Preparative and analytical extraction of pigments from brown algae with dimethyl sulfoxide. Mar Biol 1972;12:184–8. https://doi.org/10.1007/BF00350754.
[42] Ritchie RJ. Consistent sets of spectrophotometric chlorophyll equations for acetone, methanol and ethanol solvents. Photosynth Res 2006;89:27–41. https://doi.org/10.1007/s11120-006-9065-9.
[43] Sverdrup HU, Johnson MW, Fleming RH. The Oceans: their physics, chemistry and general biology, vol. 7. New York: Prentice-Hall; 1942. https://publishing.cdlib.org/ucpressebooks/view?docId=kt167nb66r;chunk.id=0;doc.view=print.
[44] Zimmerman RC, Kremer JN. Episodic nutrient supply to a kelp forest ecosystem in southern California. J Mar Res 1984;42:591–604. https://doi.org/10.1357/002224084788506031.
[45] Bell TW, Cavanaugh KC, Reed DC, Siegel DA. Geographical variability in the controls of giant kelp biomass dynamics. J Biogeogr 2015;42:2010–21. https://doi.org/10.1111/jbi.12550.
[46] Gerard VA. In situ rates of nitrate uptake by giant kelp, *Macrocystis pyrifera* (L.) C. Agardh: tissue differences, environmental effects, and predictions of nitrogen-limited growth. J Exp Mar Biol Ecol 1982;62:211–24. https://doi.org/10.1016/0022-0981(82)90202-7.
[47] Eppley RW, Renger EH, Harrison WG. Nitrate and phytoplankton production in southern California coastal waters. Limnol Oceanogr 1979;24:483–94. https://doi.org/10.4319/lo.1979.24.3.0483.
[48] Dugdale RC, Davis CO, Wilkerson FP. Assessment of new production at the upwelling center at Point Conception, California, using nitrate estimated from remotely sensed sea surface temperature. J Geophys Res Ocean 1997;102:8573–85. https://doi.org/10.1029/96JC02136.
[49] Kopczak CD, Zimmerman RC, Kremer JN. Variation in nitrogen physiology and growth among geographically isolated populations of the giant kelp, *Macrocystis pyrifera* (phaeophyta). J Phycol 1991;27:149–58. https://doi.org/10.1111/j.0022-3646.1991.00149.x.
[50] Brandt RP. Potash from kelp. Washington, D.C.: United States Department of Agriculture; 1923.
[51] Westermeier R, Möller P. Population dynamics of *Macrocystis pyrifera* (L.) C agardh in the rocky intertidal of southern Chile. Bot Mar 1990;33:363–8. https://doi.org/10.1515/botm.1990.33.4.363.
[52] Yarish Charles, Kim Jang Kyun, Lindell Scott, Kite-Powell Hauke. Developing an environmentally and economically sustainable sugar kelp aquaculture industry in southern New England: from seed to market. 2017. EEB Articles. 38, http://opencommons.uconn.edu/eeb_articles/38.
[53] Lobban CS. The growth and death of the *Macrocystis* sporophyte (Phaeophyceae, Laminariales). Phycologia 1978;17:196–212. https://doi.org/10.2216/i0031-8884-17-2-196.1.
[54] Hurd CL. Water motion, marine macroalgal physiology, and production. J Phycol 2000;36:453–72. https://doi.org/10.1046/j.1529-8817.2000.99139.x.
[55] Reed DC, Ebeling AW, Anderson TW, Anghera M. Differential reproductive responses to fluctuating resources in two seaweeds with different reproductive strategies. Ecology 1996;77:300–16. https://doi.org/10.2307/2265679.
[56] Neushul M. Studies on the giant kelp, *Macrocystis*. II. Reproduction. Am J Bot 1963;50:354–9. https://doi.org/10.1002/j.1537-2197.1963.tb07203.x.
[57] Stephens TA, Hepburn CD. A kelp with integrity: *Macrocystis pyrifera* prioritises tissue maintenance in response to nitrogen fertilisation. Oecologia 2016;182:71–84. https://doi.org/10.1007/s00442-016-3641-2.
[58] Hurd CL, Stevens CL, Lava BE, Lawrence GA, Harrison PJ. Visualization of seawater flow around morphologically distinct forms of the giant kelp *Macrocystis integrifolia* from wave-sheltered and exposed sites. Limnol Oceanogr 1997;42:156–63. https://doi.org/10.4319/lo.1997.42.1.0156.
[59] Konotchick T, Dupont CL, Valas RE, Badger JH, Allen AE. Transcriptomic analysis of metabolic function in the giant kelp, *Macrocystis pyrifera*, across depth and season. New Phytol 2013;198:398–407. https://doi.org/10.1111/nph.12160.
[60] Lindner E, Dooley CA, Wade RH. Chemical variation of chemical constituents in *Macrocystis pyrifera*. Final Rep., U.S. Naval Ocean Systems Center; 1977. San Diego.
[61] North WJ. Review of *Macrocystis* biology. In: Akatsuka I, editor. Biol. Econ. Algae. The Hague, Netherlands: SPB Academic Publishing bv; 1994. p. 447–527.
[62] Shivji MS. Interactive effects of light and nitrogen on growth and chemical composition of juvenile *Macrocystis pyrifera* (L.) C. Ag. (Phaeophyta) sporophytes. J Exp Mar Biol Ecol 1985;89:81–96. https://doi.org/10.1016/0022-0981(85)90083-8.
[63] Hepburn CD, Holborow JD, Wing SR, Frew RD, Hurd CL. Exposure to waves enhances the growth rate and nitrogen status of the giant kelp *Macrocystis pyrifera*. Mar Ecol Prog Ser 2007;339:99–108. https://doi.org/10.3354/meps339099.
[64] Gerard VA. Growth and utilization of internal nitrogen reserves by the giant kelp *Macrocystis pyrifera* in a low-nitrogen environment. Mar Biol 1982;66:27–35. https://doi.org/10.1007/BF00397251.
[65] Liu K, Kaplan IR. The eastern tropical Pacific as a source of 15N-enriched nitrate in seawater off southern California. Limnol Oceanogr 1989;34:820–30. https://doi.org/10.4319/lo.1989.34.5.0820.
[66] Sigman DM, Granger J, DiFiore PJ, Lehmann MM, Ho R, Cane G, et al. Coupled nitrogen and oxygen isotope measurements of nitrate along the eastern North Pacific margin. Global Biogeochem Cycles 2005;19:1–14. https://doi.org/10.1029/2005GB002458.
[67] Foley MM, Koch PL. Correlation between allochthonous subsidy input and isotopic variability in the giant kelp *Macrocystis pyrifera* in central California, USA. Mar Ecol Prog Ser 2010;409:41–50. https://doi.org/10.3354/meps08600.
[68] Farquhar GD, Ehleringer JR, Hubick KT. Carbon isotope discrimination and photosynthesis. Annu Rev Plant Physiol Plant Mol Biol 1989;40:503–37. https://doi.org/10.1146/annurev. pp.40.060189.002443.
[69] Riebesell U, Burkhardt S, Dauelsberg A, Kroon B. Carbon isotope fractionation by a marine diatom: dependence on the growth-rate-limiting resource. Mar Ecol Prog Ser 2000;193:295–303. https://doi.org/10.3354/meps193295.
[70] Fernández PA, Gaitán-Espitia JD, Leal PP, Schmid M, Revill AT, Hurd CL. Nitrogen sufficiency enhances thermal tolerance in habitat-forming kelp: implications for acclimation under thermal stress. Sci Rep 2020;10:3186. https://doi.org/10.1038/s41598-020-60104-4.
[71] Clendenning KA, Sargent MC. Photosynthesis and general development in *Macrocystis*. The Biology of Giant Kelp (*Macrocystis*) in California. Lehre, Germany: J. Cramer; 1971. p. 169–90.
[72] Druehl LD. Morphological and physiological responses of *Macrocystis pyrifera* to nitrate enrichment. Hydrobiologia 1984;116–117:471–4. https://doi.org/10.1007/BF00027725.